AIAA'84

AIAA-84-0012

Flow Field Studies of a Transport Airplane

M. C. Sunseri, H. C. Seetharam and M. D. Mack
Boeing Commercial Airplane Co.,
Seattle, WA

AIAA 22nd Aerospace Sciences Meeting

January 9-12, 1984/Reno, Nevada

FLOW FIELD STUDIES OF A TRANSPORT AIRPLANE

Michael C. Sunseri*
H. C. Seetharam**
Michael D. Mack***

Flight Controls Technology Research
Boeing Commercial Airplane Company
Seattle, Washington

Abstract

Experiments were conducted on a half-model transport airplane at low speeds in order to obtain a better understanding of the three-dimensional flow fields associated with the wing of a modern transport. The collected data includes force and moment measurements and complete total pressure and velocity field surveys.

The development of separated flow regions with increasing angle of attack creates dramatic changes in spanwise flow leading to the formation of part-span vortices. Flow field surveys indicate that the part-span vortices originate near the wing leading edge just above the viscous layer. When the vortices form over the wing, the magnitude of the freestream velocity component of the vortex cores is greater than the freestream velocity itself. The core velocities drop to less than the freestream level as the vortices move into the wake. The rotational characteristics of the vortices seem to persist well into the wake.

List of Symbols

b	total wing span
c	local wing chord
MAC	mean aerodynamic chord of the wing
C_L	lift coefficient
C_M	pitching moment coefficient resolved at 0.25 mean aerodynamic chord
C_P	static pressure coefficient—$(P-P_\infty)/q_\infty$
C_{P_T}	total pressure coefficient—$(P_T-P_\infty)/q_\infty$
P	local static pressure
P_T	local total pressure
P_∞	free stream static pressure
q_∞	free stream dynamic pressure
S_{FRL}	horizontal tail setting
u	longitudinal velocity component
U_{Local}	local velocity vector
U_∞	freestream velocity
v	spanwise velocity component
w	vertical velocity component
y	spanwise coordinate
α	angle of attack in degrees
α_{stall}	angle of attack for wing stall
β	crossflow angle, positive outboard
η	spanwise station, nondimensionalized with respect to semispan, $\frac{y}{b/2}$
eta	horizontal tail efficiency
eps	downwash angle

*Senior Engineer
**Senior Specialist Engineer, Associate Fellow
***Manager, Associate Fellow

Introduction

The design of a wing for a modern transport airplane is extremely complex. In order to guarantee superior cruise performance, the design engineer must finely tune features such as the planform shape, airfoil shape, spanwise thickness and camber distribution, and the wing-body nacelle integration.

The incorporation of thin airfoil sections and sweepback into the wing design process requires special care. When at incidence, thin airfoil sections possess large suction peaks that can result in leading edge separation. The turbulent boundary layer at the rear of a sweptback wing has a predominantly spanwise outflow that can trigger boundary layer separation. Either of these types of flow separation can occur at moderate angles of attack and may create an appreciable loss in airfoil lift. If this loss in lift occurs solely on the outboard wing, the airplane will experience an undesirable increase in noseup pitching moment.

Furthermore, both of the above types of separated flow may occur on the same wing simultaneously, and often include the production of part-span vortex sheets. These vortex sheets have effects on the wing wake that are in addition to those of the ordinary trailing vortices. The occurrence of part-span vortex sheets can significantly affect the downwash at the horizontal tail as well as the forces and moments of the wing. Kuchemann's work (1953)[1] gives a good account of the behavior of part-span vortex sheets arising from these mixed flows on a sweptback wing.

The ability to predict airplane performance at moderate-to-high incidence angles is of great importance to the stability and control engineer. The loss of lift, erratic changes in pitching moment, and the buffeting created at these incidence angles, are usually associated with the presence of separated flow regions located somewhere on the airplane. Therefore, the prediction of the onset and subsequent growth of separated flow regions is of considerable practical importance.

Theoretical modelling of three-dimensional flows over wings and bodies is still a developing technology. The computational routines currently in use generally predict flow field characteristics ac-

curately, as long as the flow is attached. Novel boundary layer and potential flow codes are capable of handling viscous and inviscid interactions very efficiently. Recently, Euler codes have been applied to three-dimensional flow analyses over wings; and results of these analyses have successfully predicted the development and propagation of wingtip and leading edge vortices.

Computational models must be developed and refined using the most appropriate experimental data. The available experimental data on large-aspect ratio, moderately-swept transport wings at high-incidence angles are limited in scope. For example, there is little experimental data detailing the role that part-span vortex sheets play in the performance of transport aircraft. The work of Black (1956)[2,3] on a sweptback wing verified the existence of part-span vortices and established their origin and propagative characteristics. However, the wing configuration that Black tested (leading edge sweep = 44 deg, aspect ratio = 4.3) was not the type found on modern transport airplanes.

Therefore, in view of the fact that similar experimental data for typical transport airplane configurations are extremely scarce, experimental research was undertaken to obtain data for such configurations. This paper highlights the results of the research.

Model and Test Conditions

Experiments were conducted in the 5-by-8-ft low-speed, atmospheric-entry, single-return tunnel of the Boeing Wind Tunnel Laboratories. The 0.091 scale model consisted of a wing, nacelle, half body, and horizontal tail. The model was fitted to the sidewall (fig. 1), and the model's attitude was changed by means of linkage attached to the pitch strut located outside the tunnel. Details of the model's dimensions are given in the following table:

Wing Geometry

Aspect ratio	8.85
Span	50.78 in.
MAC	12.34
1/4 c sweep	25 deg

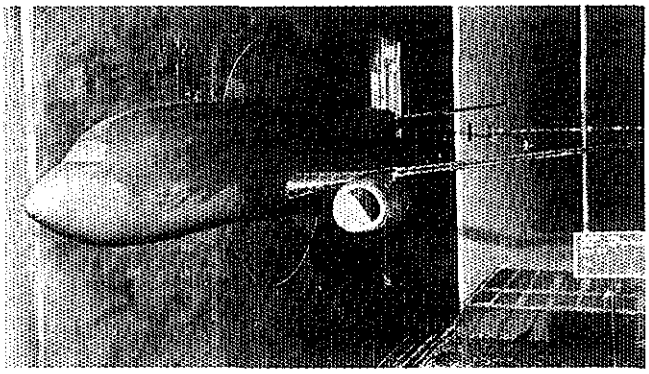

Figure 1. Model Installation

All tests were conducted at a dynamic pressure of 50 lb/ft^2, corresponding to a Reynolds number of 1.3 x 10^6 based on MAC and a Mach number of about 0.2.

Test angle of attack was varied from -4 to 24 deg with horizontal tail incidences ranging from 0 to -12 deg. Surface flow visualization, flow field surveys using a five-tube probe, and wake-imaging system surveys were conducted at selected incidences, including pre- and post-stall angles of attack.

Transition was ensured by using Carborundum grit strips on the upper and lower surfaces of the wing. Epoxy resin disks were used on the fan cowl and body to force transition.

Methods and Techniques

The model's forces and moments were measured with an external balance. Surface flow visualization tests were made employing flourescent oil flow techniques.

- Wake Imaging System. Total pressure surveys were made over the upper surface of the wing and in the wing wake using the Wake Imaging System (WIS)[4]. The WIS is a fast and easily-used measurement device that can map the onset and growth of separated flow regions. Regions that are mapped are those with a total pressure coefficient, C_{p_T}, less than 1.0.

The mapping is performed with a total pressure probe, the output of which is transduced to electrical energy that drives a multicolored light-emitting diode. The probe tip is specially made (Keil type) with an acceptance angle of greater than 40 deg. The color of the diode is a function of the total pressure level registered by the probe. The diode is mounted aft of the total pressure probe; the entire unit is mounted to a strut placed inside the wind tunnel (fig. 2). A camera mounted inside the wind tunnel is used to take a time exposure photograph of the probe/diode as it sweeps through the flow field. The resulting photographs are then digitized to facilitate analysis and presentation of the data.

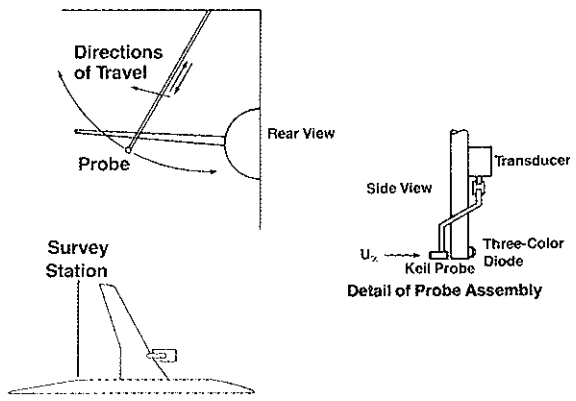

Figure 2. Wake Imaging System Details

Several WIS surveys were made at pre- and post-stall angles of attack. The locations of these surveys with respect to the wind tunnel model are illustrated in figure 3.

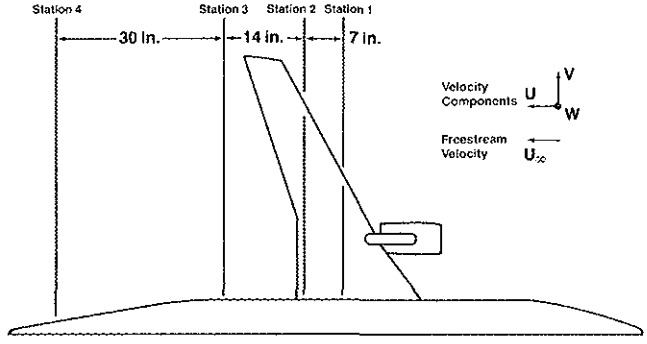

NOTE: Survey stations fixed WRT wind tunnel sidewalls. Location of survey stations WRT model varies slightly with changes in angle of attack. Here, angle of attack = 0 deg.

Figure 3. Survey Stations

• Five-Tube Probe Survey. Off-body velocity and pressure surveys were performed using a 0.25 in. dia five-tube conical probe as shown in figure 4. This probe was used to measure the rotational characteristics of the three-dimensional velocity fields over the wing and in the wake. Calibration data for the probe indicated that pitch and yaw angles of up to ±24 deg could be measured within an accuracy of 1 deg. In view of the physical dimensions of the probe, the minimum initial height was restricted to 0.5 in. from the local surface of the wing. The probe was fixed to a strut that was fixed to the tunnel ceiling; the strut had remote traversing capability horizontally and vertically in the plane perpendicular to the wind tunnel axis. The longitudinal position of the probe was set manually. Figure 3 (STA 1, 2, and 3) shows the location of the survey situations made with the five-tube probe.

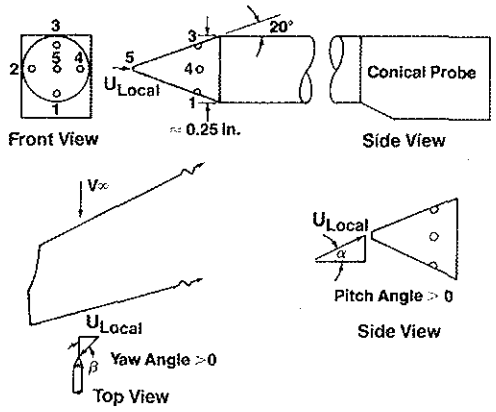

Figure 4. Five-Tube Probe Details

Results and Discussions

Forces and Moments

Figure 5 shows the lift distribution for tail off-and-on configurations. The maximum lift coefficient for all the configurations occurs between a body angle of attack of 12 to 13 deg. All configurations exhibit a gradual stall characteristic.

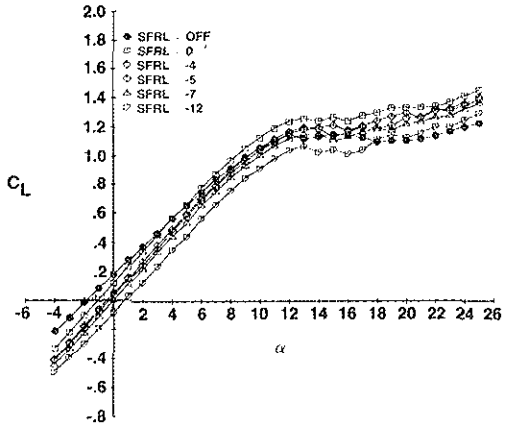

Figure 5. Lift

The longitudinal stability characteristics of the configuration are displayed in figure 6. The tail off pitching moment curve exhibits good linear characteristics up to 12 deg of angle of attack (α_{stall}). But tail on pitching moment curves show destabilizing trends below 12 deg for the case of zero horizontal tail setting. Figure 7 shows how the tail contribution to airplane pitching moment varies with the body angle of attack for the case of zero horizontal-tail incidence.

The trend in pitching moment beyond 10 deg angle of attack is very important in the assessment of stability margins and handling qualities. Two important factors are the cause of this phenomenon—the

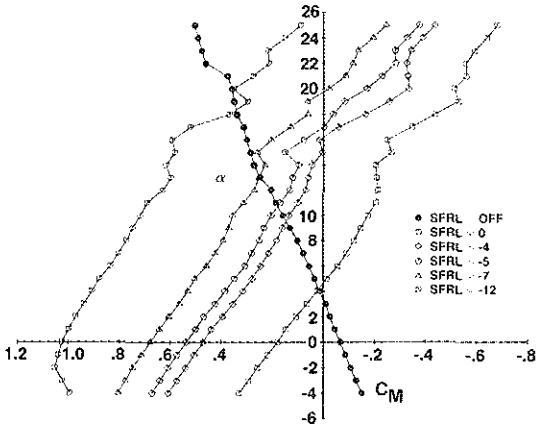

Figure 6. Pitching Moment

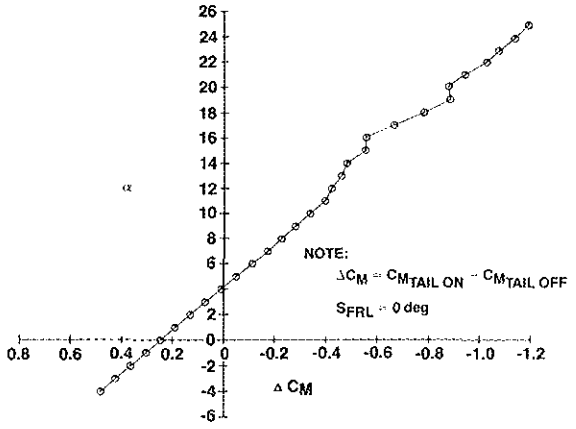

Figure 7. Tail Contribution to Pitching Moment, $S_{FRL} = 0$ deg

wing performance at high angles of attack and the associated downwash field, and low-energy wake generated by the wing. The wing performance at high angles of attack will be discussed in the next section on flow visualization.

From the lift and pitching moment data, average downwash and relative tail efficiency were computed and shown in figure 8. The average downwash field shows a generally linear trend in the range of angles of attack of 2 to 12 deg and becomes highly nonlinear at higher angles of attack. The tail efficiency begins to drop at about 12 deg angle of attack as the tail enters the low-energy wake from the stalled wing.

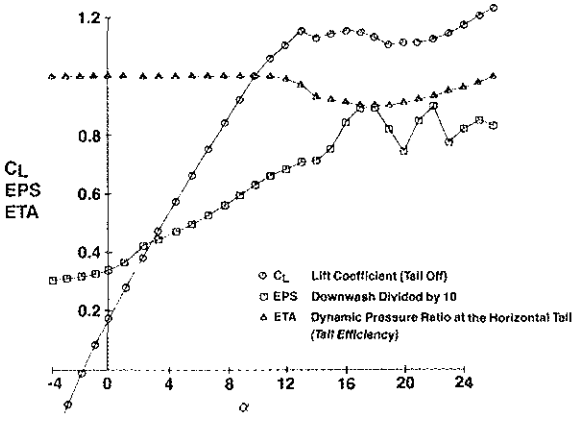

Figure 8. Lift, Downwash, and Tail Efficiency

Surface Flow Visualization

The force data recorded at angles of attack of 10 deg and above are important in evaluating the stability and handling qualities of the airplane. Surface flow visualization provides a useful clue to understanding the stall onset and post-stall characteristics.

The results of the fluorescent oil flow testing performed at 10, 12, 14, and 16 deg angle of attack are shown in figures 9, 10, 11, and 12, respectively. The figures illustrate the development of separated flow over the wing's upper surface.

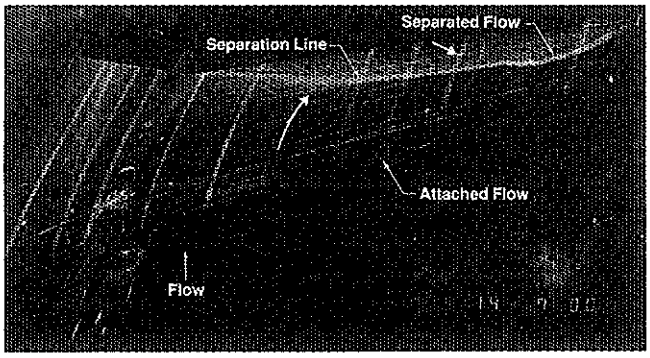

Figure 9. Fluorescent Oil Flow, α = 10 deg

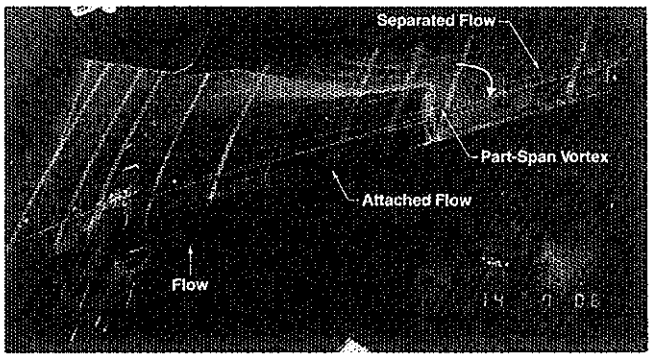

Figure 10. Fluorescent Oil Flow, α = 12 deg

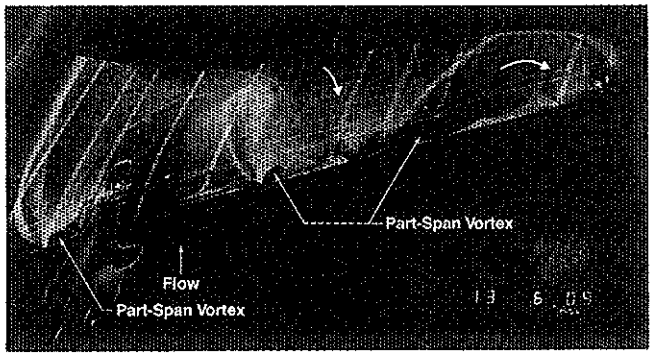

Figure 11. Fluorescent Oil Flow, α = 14 deg

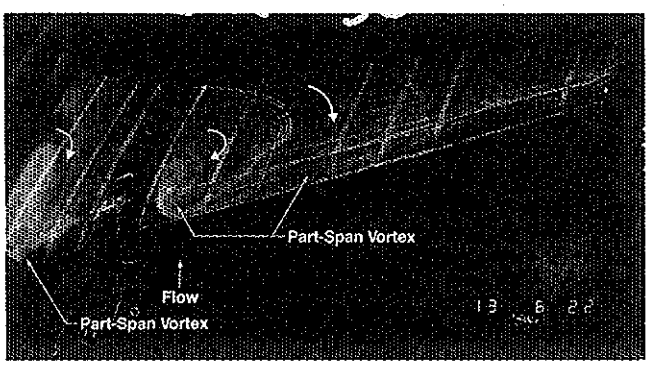

Figure 12. Fluorescent Oil Flow, α = 16 deg

At 10 deg angle of attack (fig. 9), trailing edge separation originates outboard of the nacelle strut and extends out to the wingtip. A separation line divides the attached flow region upstream of the line from the separated flow region downstream of the line. The fluorescent oil flows primarily outboard in the separated flow region (oil flow directions are indicated by the white arrows in the figure).

Figure 10 shows the upper surface flow conditions at 12 deg angle of attack (α_{stall}). The flow pattern has changed dramatically compared with that in the previous figure. The flow from approximately 75% semispan out to the wingtip has separated at the leading edge. A spiral-shaped pattern has been created at the junction of the trailing edge separation line and the separated flow at the leading edge (75% semispan). Oil flows into this spiralling region (1) from the separated flow region, (2) outboard along the trailing edge separation line, and (3) inboard along the wing leading edge.

Upper surface flow conditions for the post-stall angle of attack of 14 deg are shown in figure 11. The flow patterns indicate that there are now three leading-edge (part-span) vortex systems present on the wing. The centers of the systems are located at 12%, 50%, and 85% semispan.

The results of the oil flow at 16 deg angle of attack are shown in figure 12. The centers of the three vortex systems have all moved inboard with the increase in angle of attack. The vortex systems are now located at 8%, 35%, and 55% semispan. The vortex systems at 8% and 35% semispan are extensive.

Total Pressure Surveys With WIS

Analysis of the surface flow visualization and force data helped in the choice of test conditions to carry out the total pressure surveys. Longitudinal stations were set up over the wing, in the near wake and at the 0.25 MAC of the horizontal tail station (fig. 3). The WIS provided a graphic picture of total pressure loss regions dominated by viscous separated flow fields. The results are presented to illustrate—

1. The development of total pressure loss regions in the near wake (STA 3, of fig. 3) with angle of attack from the pre-stall α = 10 deg to post-stall α = 16 deg (figs. 13 to 16)

2. Longitudinal development of the total pressure loss regions at α = 16 deg (fig. 17)

3. The vertical and horizontal extent of total pressure loss region at the horizontal tail location (figs. 18 to 23)

Surveys at Body Station 3: (figures 13 to 16). Near wake total pressure surveys at 10 deg angle of attack (fig. 13) indicate three well-defined total pressure loss regions of $C_{P_T} < 0.3$, over the wing (one inboard and two outboard of nacelle). The pressure signature due to the nacelle and strut wake can also be seen. The surface flow visualization (fig. 9) indicates trailing edge separation outboard of the nacelle. But the total pressure survey shows a substantial total pressure loss region extending from 80% semispan to about 100%. This is possibly due to strong gradients in the spanwise flow, which progressively thickens the boundary layer outboard. Also, notice a well-defined trailing vortex core from the wingtip with substantial total pressure loss. At an angle of attack of 12 deg (α stall), the regions of total pressure loss grow larger (fig. 14). The nacelle wake is now merged with the wing wake. The signature of the tip vortex core is larger. At post-stall angles of 14 and 16 deg, the total pressure maps indicate dramatic growth of total pressure loss regions all across the span (figs. 15 and 16).

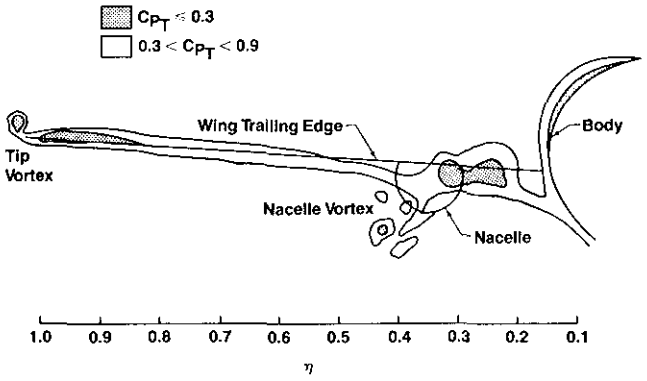

Figure 13. Digitized Total Pressure Map, Station 3, α = 10 deg

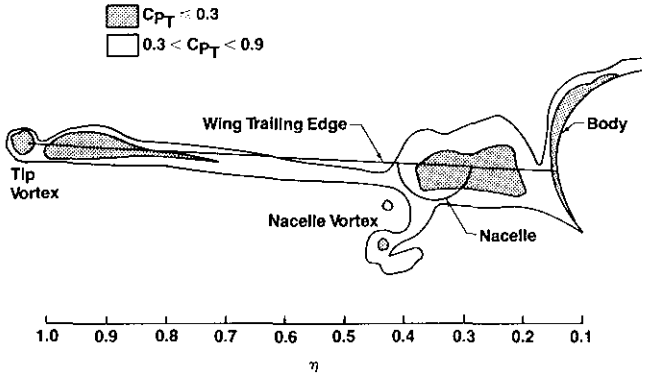

Figure 14. Digitized Total Pressure Map, Station 3, α = 12 deg

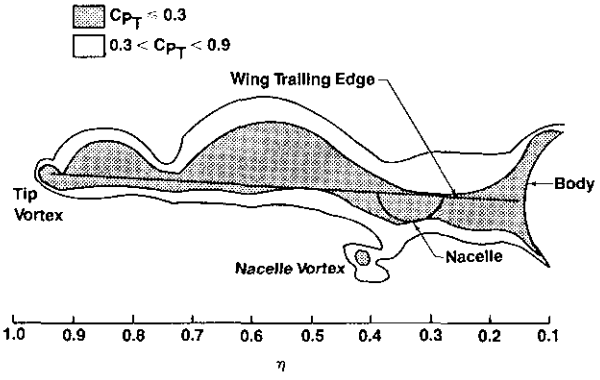

Figure 15. Digitized Total Pressure Map, Station 3, α = 14 deg

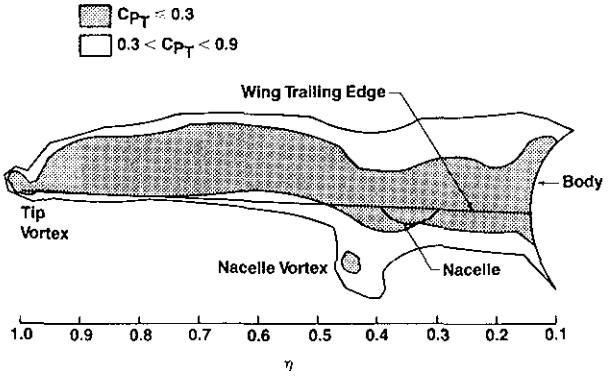

Figure 16. Digitized Total Pressure Map, Station 3, α = 16 deg

Surveys at α = 16 deg: (figure 17). The body attitude of 16 deg was selected from the examination of force and flow visualization data for further investigation. The tail on pitching moment curves (fig. 6) indicate a recovery from the first pitchup loop. Also the flow visualization (fig. 12) indicates part-span vortex systems originating near the wing leading edge.

Total pressure surveys were made at several longitudinal stations (fig. 17), but only three survey station maps are shown here for the purposes of the present discussion. Total pressure surveys over the wing indicate considerable thickening of the viscous regions, particularly inboard of the nacelle. Station 1 indicates a very shallow region of total pressure loss outboard of the nacelle. The nacelle strut acts as a boundary layer fence and prevents local spanwise flow. The effect of the nacelle strut is noticeable at all survey stations. This isometric composite of the surveys presents a graphic picture of the progressive thickening of the low-energy regions over the wing and into the wake.

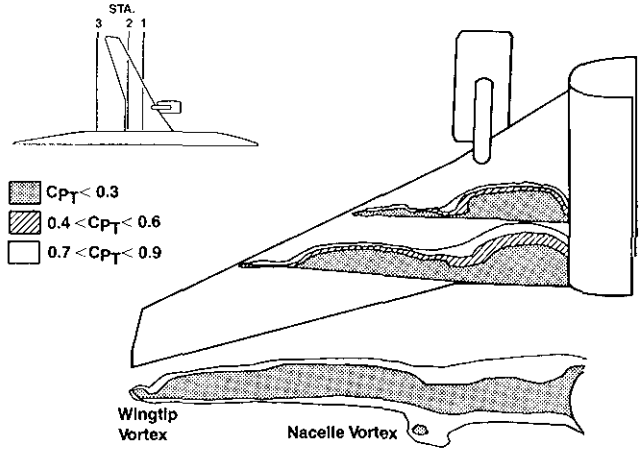

Figure 17. Development Total Pressure Field, α = 16 deg

Surveys at 0.25 MAC of Horizontal Tail: (figures 18 to 23). In order to understand the performance of a horizontal tail under the influence of the wake produced by the wing, body, and nacelle, total pressure surveys were carried out at the 0.25 MAC horizontal-tail station at several body incidences. The choice of body incidences was made from the pitching moment data (figs. 6 and 7). It is seen from the figures that the departure from linearity occurs at about 10 deg, which indicates the onset of a gradual loss of stability. Between 10 and 21 deg, the airplane goes through two cycles of pitchup due to the deterioration of wing performance (that is, massive flow separation) and the effects of the wing wake and vortical flows from the body, nacelle, and wing on the horizontal tail.

Figures 18 through 23 show the development of total pressure loss regions at the horizontal-tail for angles of attack of 10 through 21 deg. The total pressure maps were obtained with the horizontal tail removed. The position of the horizontal tail is shown for reference. The pressure signature from the wing wake for α = 10 deg (fig. 18) indicates moderate total pressure loss and significant interaction with the horizontal tail. It is interesting to note that the nacelle wake is situated well below the main wing wake and that the tip vortex is well defined.

At α = 12 deg (fig. 19), the thickness of the inboard and outboard wakes grows and most of the horizontal tail is submerged in the low-energy wake from the inboard wing. Note again that the total pressure is still moderate (C_{P_T} = 0.7 to 0.9), which indicates a dynamic pressure loss of about 20% relative to the free stream. The nacelle

NOTE: The Legend In Figures 18-23 Should Read $C_{P_T} < 0.3$; $0.3 < C_{P_T} < 0.9$

wake is still isolated from the wing wake, due to the strong downwash field generated by the wing, and has moved closer to the tip of the horizontal tail.

Post-stall total pressure maps (figs. 20 to 22) indicate massive total pressure loss, resulting from wing flow separation. The horizontal tail experiences a substantial dynamic pressure loss and rapid changes in downwash. Notice also that the nacelle wake merges with the wing wake. As the angle of attack is increased, the nacelle wake migrates from below the horizontal tail to above the tail. The average downwash at the tail (fig. 8) increases as the nacelle wake approaches the tail and decreases when the nacelle wake moves above the tail.

For an angle of attack of 21 deg (fig. 23), the entire wing wake moves up and away from the horizontal tail; only the inboard region of the horizontal tail is under the influence of the low energy wake. Figure 8 shows that the tail efficiency is improving in this region.

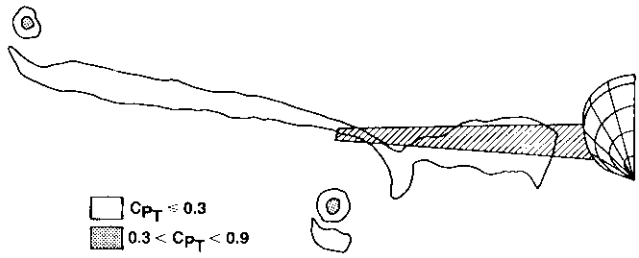

Figure 18. Total Pressure Field at Horizontal Tail Station, α = 10 deg

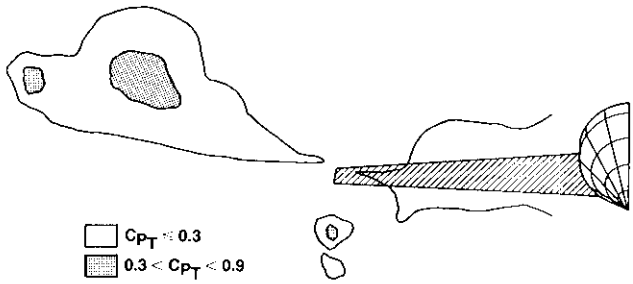

Figure 19. Total Pressure Field at Horizontal Tail Station, α = 12 deg

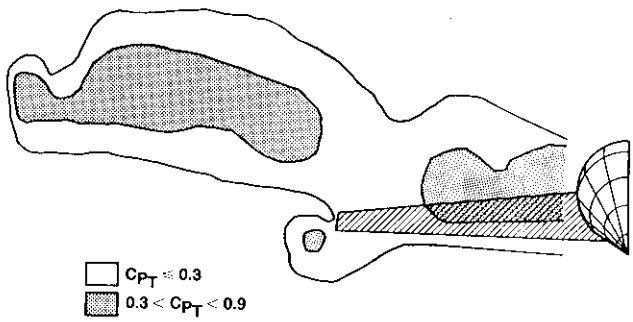

Figure 20. Total Pressure Field at Horizontal Tail Station, α = 14 deg

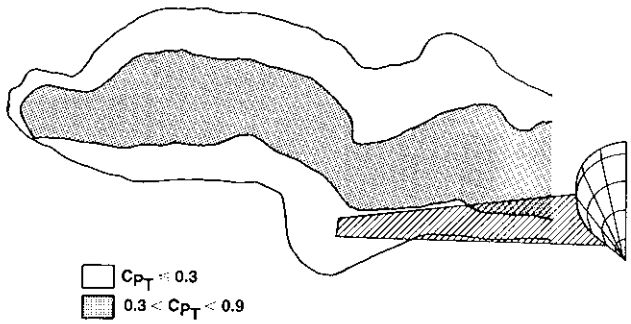

Figure 21. Total Pressure Field at Horizontal Tail Station, α = 16 deg

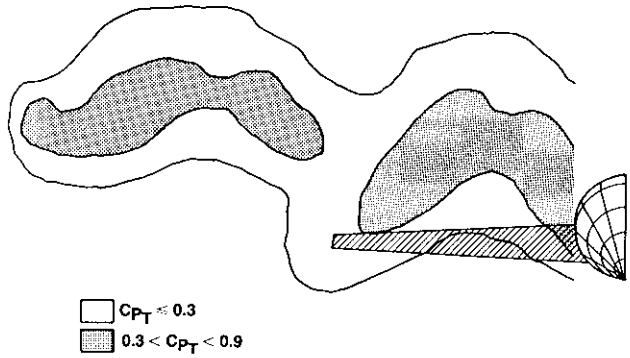

Figure 22. Total Pressure Field at Horizontal Tail Station, α = 18 deg

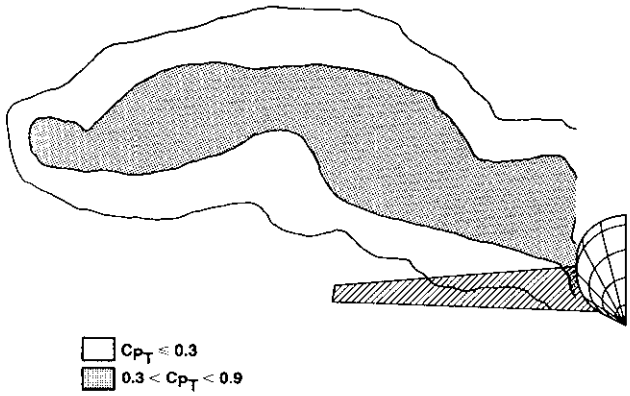

Figure 23. Total Pressure Field at Horizontal Tail Station, α = 21 deg

Five-Tube Probe Measurements

Figures 24 through 26 show the pitch and crossflow data obtained at survey stations 1 through 3, respectively. The data, plotted in vector format, indicate the existence of several areas of rotational flow. At least four regions of rotational flow occur in the near-wake data of figure 26. Part-span vortices are responsible for the rotational flow in two of these regions (50 and 80% semispan). Of the two remaining regions, one area is caused by the wingtip vortex (100% semispan) and one area is due to a vortex created by the nacelle (45% semispan).

Vorticity contours were calculated using the velocity data of figures 24 through 26. The results of these calculations are shown in figure 27. Two part-span vortex systems form over the wing and propagate into the wake. Vortex 1 in figure 26 appears to have its origin at the wing leading edge, however, the origin of Vortex 2 cannot be found with the data available here. Each vortex system travels slightly outboard as it moves from the trailing edge into the wake.

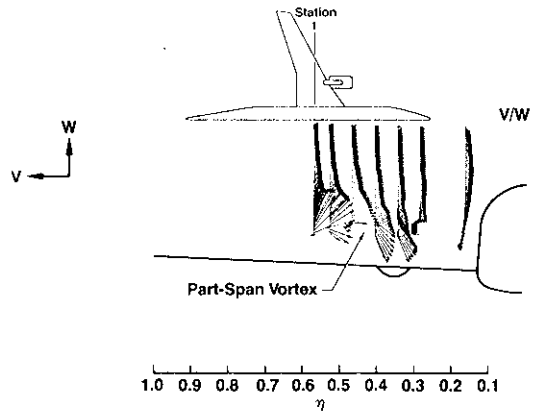

Figure 24. Pitch and Crossflow Velocity Vector Field, Station 1, α = 16 deg

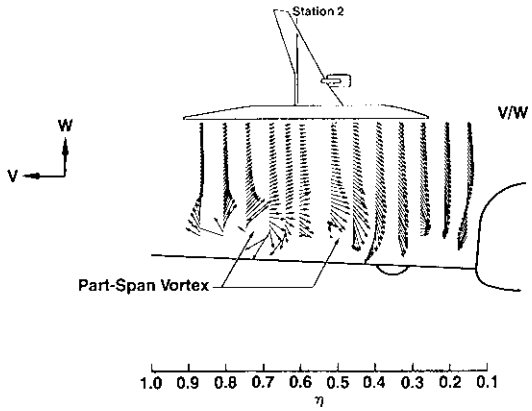

Figure 25. Pitch and Crossflow Velocity Vector Field, Station 2, α = 16 deg

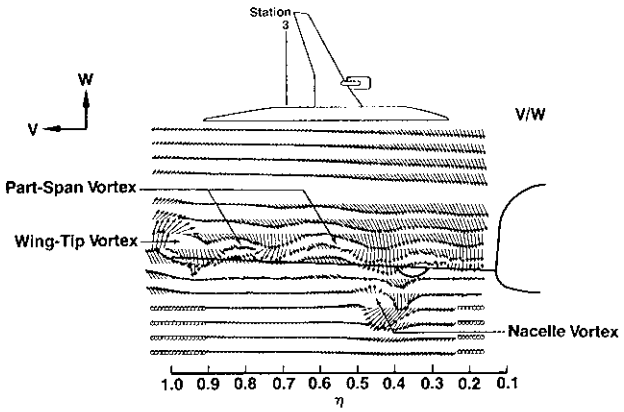

Figure 26. Pitch and Crossflow Velocity Vector Field, Station 3, α = 16 deg

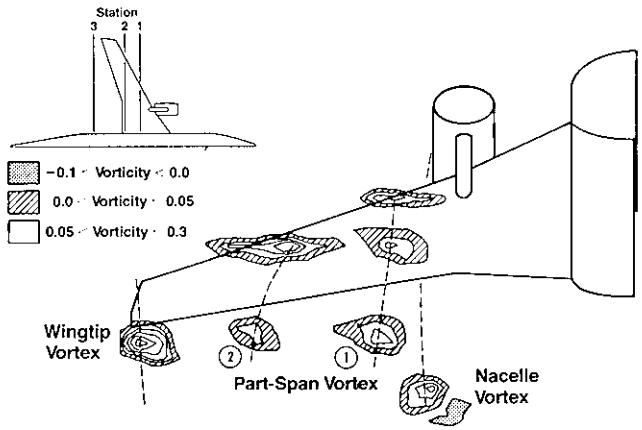

Figure 27. Vorticity Field, α = 16 deg

The wingtip and nacelle vortices are also shown in figure 27. Note that the nacelle vortex is actually a system of two, counter-rotating vortices. The strongest vortex of the nacelle vortex system rotates clockwise as viewed in this figure. The wingtip vortex and the part-span vortices also rotate clockwise. This direction corresponds to the direction of the air circulating around the wing induced by the pressure difference between the wing's upper and lower surfaces.

No significant vorticity was found in the region between the nacelle and the side of the body either over the wing or in the near wake.

Longitudinal velocity contours calculated using the five-tube probe data are shown in figure 28. The longitudinal velocity component data were normalized by the tunnel freestream velocity.

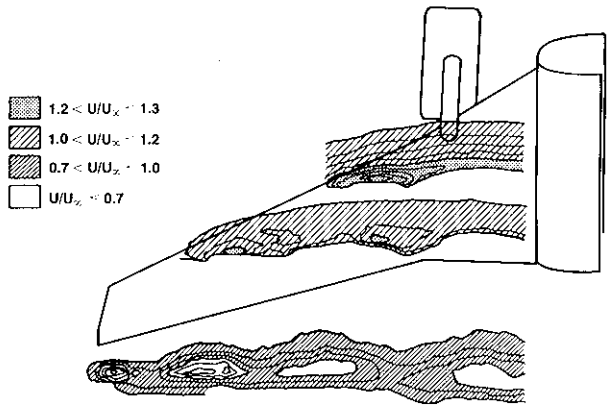

Figure 28. Longitudinal Velocity Field Contours, α = 16 deg

The locations of the core regions of the longitudinal velocity contours correspond to the locations of the centers of the vortices of the vorticity plots of figure 27, that is, the cores of the longitudinal velocity contours are the cores of the part-span and wingtip vortices.

Over the wing, the longitudinal velocity of the part-span vortex cores is greater than the freestream velocity itself. It is interesting to note that the vertical location of the vortex core appears to be just above the total pressure loss region (viscous layer). Obviously, the WIS did not detect the existence of part-span vortices. The figure shows that the core of vortex 1 is up to 30% greater than freestream velocity. However, as the part-span vortices move into the wake, the longitudinal velocities of the vortex cores drop below freestream velocity.

Conclusions

- Large vortical flows developing from part-span vortex sheets form above the stalled wing of the transport configuration tested.
- Above the wing, the longitudinal velocities of the cores of these vortices are greater than freestream. The longitudinal velocities of the vortex cores drop to less than freestream velocity in the wake.
- The centers of the vortical flows ride just above the viscous layer.
- There is a total pressure loss in the wake associated with the creation and propagation of the part-span vortices. Although the dynamic pressure loss decreases with increasing longitudinal distance from the wing's trailing edge, the complex, swirling motion of flow field seems to persist well into the wake.
- The Wake Imaging System maps, particularly at the horizontal tail stations, provide a graphic picture of the total pressure loss field, with increasing angle of attack. This is very useful in understanding the performance of the horizontal tail due to complex wing-nacelle-body wake development and interaction.
- The Wake Imaging System, five-tube probe, and surface-flow visualization techniques along with the force, moment, and surface pressure measurements are all necessary tools to be used in gaining an understanding of these complex, separated flow phenomena.

References

1. Kuchemann, D., "Types of Flow on Swept Wings," Journal of Royal Aeronautical Society, November 1953.

2. Black, J., "Flow Studies of the Leading Edge Stall on a Swept-Back Wing at High Incidence," Journal of Royal Aeronautical Society, January 1956.

3. Black, J., "A Note on the Vortex Patterns in the Boundary Layer Flow of a Swept-Back Wing," Journal of Royal Aeronautical Society, April 1952.

4. Crowder, J. P., "Quick and Easy Flow-Field Surveys," Aeronautics and Astronautics, October 1980.